Silica cementation history of the Ediacara Member (Rawnsley Quartzite, South Australia): Insights from petrographic and *in situ* oxygen isotopic microanalyses

Silvina Slagter[1,*], Lidya G. Tarhan[1], Tyler B. Blum[2], Mary L. Droser[3], John W. Valley[2]

[1]*Department of Earth and Planetary Sciences, Yale University, New Haven, CT 06511, USA*

[2]*WiscSIMS Lab, Department of Geoscience, University of Wisconsin, Madison, WI, 53706-1692, USA*

[3]*Department of Earth and Planetary Sciences, University of California, Riverside, Riverside, CA 92521, USA*

[*]*Corresponding author*

Keywords: oxygen isotopes, Ediacara Biota, fossilization, silica, diagenesis

Final published paper:

Slagter S, Tarhan LG, Blum TB, Droser ML, Valley JW (2024) Silica cementation history of the Ediacara Member (Rawnsley Quartzite, South Australia): Insights from petrographic and in situ oxygen isotopic microanalyses. Precam Res. 402, 107288

ABSTRACT

The Ediacara Member of the Rawnsley Quartzite in South Australia is characterized by exceptional preservation of soft-bodied organisms as casts and molds in sandstones. To understand the timing of silica cementation and the relationship between fossilization and the broader diagenetic history of the Ediacara Member, we used a combination of electron backscatter diffraction (EBSD) analyses, cathodoluminescence (CL) imaging and *in situ* analysis of oxygen isotopes ($\delta^{18}O$) by secondary ion mass spectrometer (SIMS) of detrital quartz grains and authigenic quartz overgrowths in sandstone samples hosting Ediacara Biota macrofossils.

We find that the mean $\delta^{18}O$ value of overgrowth quartz (OQ) from analyzed samples of the Ediacara Member is 18.48 ± 2.5‰ (1SD with a range of 7.5‰–26.7‰) and quartz overgrowths are systematically zoned, with decreasing $\delta^{18}O$ values outward from the quartz grains, consistent with progressive and continued cementation. These results suggest an early diagenetic initiation of silica cementation adjacent to the quartz grain boundaries, followed by later stages of cementation more distal from grain boundaries and likely under the influence of higher-temperature burial diagenetic processes. These data support the idea that early silica precipitation from silica-rich seawater may have played a critical role in the fossilization of Earth's earliest animal ecosystems, and better elucidate the diagenetic history of a key Ediacaran fossil deposit that has uniquely shaped understanding of the ecology, diversity, paleoenvironment, and preservation of early complex, macroscopic life.

1. INTRODUCTION

The Ediacara Biota represents the earliest fossil record of communities of complex, macroscopic, and multicellular organisms. Fossils of these soft-bodied organisms are extraordinarily well-preserved as casts and molds in sandstones (e.g., Gehling, 2000; Narbonne, 2005), in what has been termed the Ediacara style (Tarhan et al., 2016). Some of the best-characterized and richest Ediacara fossil deposits, such as the Ediacara Member (Mb.) of the Rawnsley Quartzite at the Nilpena Ediacara National Park (NENP) in South Australia, are preserved in fine- to medium-grained quartz-feldspar arenites (e.g., Tarhan et al., 2016, 2017). However, the mechanisms responsible for the formation of these moldic fossils remain debated. Some studies have proposed that precipitation of iron minerals (e.g., Gehling, 1999; MacGabhann et al., 2019) or the presence of either detrital (Wade, 1968; Bobrovskiy et al., 2019) or authigenic (Laflamme et al., 2011) clay minerals may have facilitated Ediacara-style preservation though recent work has highlighted the late-stage nature of ferruginous bed coatings and absence of clay minerals from the fossiliferous Ediacara Member (Tarhan et al., 2016, 2018). Conversely, sedimentary and petrographic evidence (e.g., resedimented sandstone rip-up clasts, extensive quartz cements, the near-absence of other mineral phases, and limited pressure-solution features), as well as geochemical data (e.g., quartz-hosted Ge/Si signatures), have recently been used to interpret an early diagenetic silica cementation history for the fossiliferous Ediacara Member at NENP (Tarhan et al., 2016, 2017). In this framework, early-forming silica cements are inferred to have facilitated early lithification of sands surrounding episodically buried Ediacara macroorganism and microbial matground seafloor communities, facilitating rapid moldic templating of organism morphologies prior to soft-tissue decay (Tarhan et al., 2016; Slagter et al., 2022). This style of fossilization has been proposed to be linked to global marine conditions characterized by elevated dissolved silica (DSi) concentrations before the emergence of silica-biomineralizing organisms in the early Phanerozoic (Siever, 1992). Likewise, silica-rich sedimentary deposits such as early-forming cherts and silicilytes (e.g., Kidder and Tomescu, 2016; Dong et al., 2015; Ramseyer et al., 2013), and other silica-associated modes of fossilization, such as Bitter Springs-style preservation of organic-walled microfossils, have been interpreted to reflect elevated seawater DSi concentrations across this interval (Butterfield, 2003).

Further characterization of Ediacara fossils from the NENP—coupled with decay experiments involving experimental silicification of a range of soft-bodied Ediacara-analogue organisms, potentiometric titration analyses and Fourier transform infrared spectroscopy—have resulted in a taphonomic model suggesting that reactions between porewater silicic acid and organic functional groups in the tissues and cell walls of buried macroorganisms and microbial mats facilitated early diagenetic silica cementation (Tarhan et al., 2016; Slagter et al., 2021; Slagter et al., 2022). In particular, this work has highlighted the potential importance of organically mediated silica sorption reactions—fueled by the presence of silica-reactive hydroxyl, phosphoryl, carboxyl, and amino groups within macroorganism tissues and microorganism cells—in catalyzing amorphous silica precipitation and thus moldic fossilization (Slagter et al., 2021, 2022). Under this model, amorphous silica cements would have subsequently transformed to more stable and crystalline silica phases (i.e., quartz) during later stages of diagenesis (Slagter et al., 2021).

However, direct and independent assessment of the paragenetic and burial history of the Ediacara Mb., including whether discrete stages of cementation occurred and the original mineralogy (e.g., amorphous, opaline or quartz) of these silica precipitates, has been hampered by the nearly monomineralic nature of the Ediacara Mb. at NENP and limited independent constraints on the burial history of either NENP or other key fossiliferous Ediacara Mb. localities. We address this by using cathodoluminescence (CL) imaging of syntaxial quartz overgrowths and quartz grains coupled with petrographic microscopy and electron backscatter diffraction imaging in fossiliferous samples from the Ediacara Mb., a deposit that has played an outsized role in reconstructing not only the diversity, ecology and environmental distribution of Ediacara Biota macroorganisms but also their taphonomy, and where competing hypotheses for the mechanisms responsible for Ediacara-style fossilization first originated. Additionally, we employ *in situ* secondary ion mass spectrometer (SIMS) oxygen isotope measurements ($\delta^{18}O$) of quartz overgrowths to further elucidate geochemical conditions under which these cements precipitated and thus facilitate reconstruction of the diagenetic history of these strata (e.g., Heck et al., 2011). Using this approach, we find that quartz overgrowths in the fossiliferous Ediacara Mb. record an early diagenetic stage of cement precipitation, likely sourced from seawater and shallow marine porewaters (cf. McBride, 1989), followed by continuous precipitation of silica-rich cements that we interpret to have formed during later stages of burial diagenesis.

2. METHODS

2.1 Geological and paleontological background

The Rawnsley Quartzite is the uppermost Ediacaran unit in the Neoproterozoic–middle Cambrian succession of the Adelaide Superbasin of South Australia (Gehling, 2000; Lloyd et al., 2020). The Ediacara Member consists of tens to hundreds of meters of quartzofeldspathic arenite interpreted to have been deposited across a range of shallow marine storm-influenced and deltaic settings (e.g., Gehling and Droser, 2013; Reid et al., 2020). The fossiliferous Ediacara Mb. is additionally bracketed by hundreds of meters of lithologically similar strata (Gehling and Droser, 2013).

Here, we focus upon the two most fossiliferous facies of the Ediacara Mb., as characterized at NENP: the Oscillation-Rippled Sandstone (ORS) Facies and the Planar-Laminated and Rip-Up Sandstone (PLRUS) Facies (Droser et al., 2017; Tarhan et al., 2017). The ORS Facies is characterized by thin-bedded, oscillation- and interference-rippled, fine- to medium-grained feldspathic quartz arenites interpreted to have been deposited near fair-weather wave base (Gehling and Droser, 2013; Tarhan et al., 2017; Droser et al., 2022; Tarhan et al., 2022). Ediacara fossils occur as hyporelief external, internal, and composite molds and, less commonly, epirelief casts in these facies (Fig. 1; e.g., Tarhan et al., 2015; Droser et al., 2020; Surprenant et al., 2020; Slagter et al., 2022). The PLRUS Facies consists of laterally continuous, planar-laminated, fine-grained sandstone beds that occasionally bear tool-marked lower surfaces and are interpreted to have been deposited below storm wave base as part of an incised valley-fill succession (Gehling and Droser, 2013; Paterson et al., 2017; Tarhan et al., 2017). Fossils of the PLRUS facies also occur as hyporelief external and internal molds (e.g., Droser et al., 2020).

Fossils preserved in the analyzed NENP samples include the Ediacara body fossils *Dickinsonia*, *Coronacollina*, tubular fossils *Funisia* and *Plexus*, *Aspidella* holdfasts of frondose organisms (Fig. 1a), and the octaradially spiraling taxon *Eoandromeda* (Fig. 1b); as well as *Helminthoidichnites* trace fossils recording undermat-mining behavior by bilaterian animals. These samples also include a variety of textured organic surface (TOS) morphologies, recording interactions between mats of densely aggregated micro- and macro-organisms and hydrodynamic and sedimentary processes (Fig. 1). The analyzed fossiliferous material is associated with and representative of excavated beds, successions and sites for which the sedimentology, paleoecology and taphonomy have been extensively characterized at the field scale, including beds TC-MM3, STC-B, STC-H and the 1T succession of the ORS Facies as well as bed MAB and associated exposures in the PLRUS Facies (Table S1; cf. Droser et al., 2019). Samples were collected over the course of several field seasons for petrographic and geochemical analyses, including optical petrography, scanning electron microscopy (SEM), and electron microprobe analyses (EPMA). Petrographic, SEM and EPMA observations, in turn, were used to select areas for SIMS sample preparation and analyses. Fossil samples analyzed for this study are held in the collections of the South Australian Museum.

2.2 Electron microscope and electron microprobe imaging

Detrital quartz grains (DQ) and quartz overgrowth cements (OQ) were identified by cathodoluminescence (CL), backscattered electron (BSE), and secondary electron (SE) imaging. Areas for imaging and SIMS analyses were identified in thin sections and ~1 cm^3 polished chips mounted in epoxy; a total of 28 areas of ~0.25 mm^3 each were subsequently analyzed by SIMS. Images of detrital quartz grains and their corresponding authigenic quartz overgrowths were collected using a JEOL JXA-8530F Field Emission Gun (FEG) electron probe microanalyzer (EPMA) at the Yale Electron Microprobe Laboratory, Department of Earth and Planetary Sciences, Yale University, with an accelerating voltage of 15 kV and beam current of 20 nA. CL and SE images were also taken both prior to and following SIMS analyses with a Gatan Pana CL/F imaging system on a Hitachi S-3400 N Scanning Electron Microscope (SEM) at the University of Wisconsin, Madison using an accelerating voltage of 15 kV. Post-SIMS-analysis SE images were collected to examine ablation pit morphology and confirm the petrographic character of material analyzed by SIMS. Additionally, BSE, CL, SE, and EDS images were collected in the Yale SEM Laboratory at the Earth Material Characterization Center in the Department of Earth and Planetary Sciences, Yale University, using a Hitachi SU700 with an accelerating voltage of 10 kV.

2.3 Oxygen isotope analyses

Oxygen isotope ($\delta^{18}O$) and raw $^{16}OH/^{16}O$ data were acquired at the Wisconsin SIMS Laboratory (WiscSIMS) using a CAMECA IMS 1280 large-radius multicollector ion microprobe, following the procedures of Kita et al. (2009) and Wang et al. (2014). Oxygen isotope analyses utilized a

~2 nA primary beam of $^{133}Cs^{+}$ ions, generating analytical pits of ~10–12 μm diameter. The typical intensity of the secondary $^{16}O^{-}$ beam was 2.5×10^{9} counts per second. Individual analyses lasted approximately 3 min, including pre-sputtering of the gold-coated surface (10 s), automatic centering of the secondary ion beam in the field aperture using high-voltage deflectors (60 s), and 20 cycles of 4-second integrations of oxygen ion measurements. The $^{16}O^{-}$, $^{16}OH^{-}$ and $^{18}O^{-}$ ions were all collected with Faraday cups. Hydride interferences at mass 18 were resolved at a mass-resolving power (MRP) of 2200, and a MRP of ~5000 was used for mass 17 to resolve $^{16}OH^{-}$ from $^{17}O^{-}$. Each set of sample measurements was bracketed by eight analyses of the UWQ-1 quartz standard, four before and four after every 10 to 16 sample analyses. The mean of these bracketing standard values was used to determine the raw ratio of $^{16}OH/^{16}O$ and the instrumental bias for $\delta^{18}O$ based on the calibrated UWQ-1 value; sample precision was estimated from the 2SD of bracketing standards (Kita et al., 2009; Kelly et al., 2007). Oxygen isotope ($\delta^{18}O$) results are reported in reference to Vienna Standard Mean Ocean Water (VSMOW).

Following SIMS analyses, both pit imaging and review of internal metrics (e.g., standard error and relative yield) were used to evaluate data quality and the potential for irregular sputtering processes that can result in inaccurate $\delta^{18}O$ measurement (Kita et al., 2009; Valley et al., 2009). The morphology of sputtering pits was examined using secondary electron (SE) imaging, as described above. Data from pits identified as morphologically 'irregular'—e.g., transecting cracks, cavities, or inclusions (e.g., Cavosie et al., 2005)—are indicated in the Appendix but were excluded from subsequent analyses and discussion of SIMS oxygen isotope data. Internal standard error, yield and $^{16}OH/^{16}O$ values were considered relative to the behavior of standards; for this session, sample measurements with 2SE>0.38 ‰ for $\delta^{18}O$ (SE=standard error), yield

<0.98 or >1.04 [(cps(sample)/ cps(standards)], or background-corrected $^{16}OH/^{16}O$ >1x10^{-4} were also excluded (dataset available in Appendix). This set of criteria represents a highly conservative assessment of data quality and provides confidence that observed trends do not reflect analytical artefacts. Using these criteria, 29 of a total of 508 measurements (<6%) were discarded and not further considered (see Appendix). All data were spatially visualized using the 3.26 version of the QGIS software (Linzmeier et al., 2018) and are reported in Figs. 4–6, S1-S5 and the Appendix.

2.4 Electron backscatter diffraction (EBSD) analyses

Electron microscope imaging and crystallographic orientation mapping were performed using a Hitachi SU7000 SEM in the SEM Laboratory of the Earth Material Characterization Center in the Yale Department of Earth and Planetary Sciences. Targeted areas were first selected and identified by using the Hitachi SU7000's BSE- and CL-imaging capabilities. The areas were then subjected to crystallographic orientation mapping using a Gatan Monard 450 CL system attached to an Oxford Instrument EBSD system, which has a Symmetry detector and Aztec software package. The following conditions for EBSD mapping were applied: a working distance of 17 mm, 20 kV accelerating voltage, and 70° stage tilting.

3. RESULTS

Examination of petrographic, SEM and EPMA images indicates the presence of extensive quartz overgrowths, including triple junctions, limited grain-to-grain contacts, and minor occurrences of pressure-solution features (such as sutured boundaries of detrital quartz grains) in the analyzed NENP samples (Fig. 2). When examined petrographically using light microscopy, these overgrowths appear syntaxial (i.e., optically continuous with detrital grains), as is characteristic of many Neoproterozoic and lower Paleozoic quartzose sandstones (McBride, 1989). The majority of CL and SE images show clear zonation of OQ, including instances of serial, concentric zonation proximal to DQ grain boundaries (Fig. 3; cf. Sibley and Blatt, 1976; Pittman, 1979; Pollington et al., 2011). Irregularly shaped overgrowths (i.e., an absence or paucity of clear concentric patterns), either proximal to or distal from detrital grain margins, were observed to be uncommon (Figs. S1c, S2c, S3b, S4a, S5c).

To further investigate the formation pathways and crystallinity of silica overgrowths (e.g., Lynne et al., 2007; French and Worden, 2013), EBSD analyses were performed. The EBSD images were compared with optical photomicrographs, SEM-BSE images, and CL images of the same sample regions. These data indicate that, despite the syntaxial appearance of these cements when viewed using light microscopy, the crystallographic orientations of paired quartz grains and overgrowths within the studied sample areas are not consistently aligned. Although in some instances paired detrital grains and overgrowths possess similar orientations, these are also commonly dissimilar (Fig. 4, Figs. S6-S10). The term "syntaxial" is variably employed, even within the mineralogical community (e.g., Dickson, 2023); we hereafter refer to cements as syntaxial if they appear optically continuous with detrital grains when viewed using light microscopy although, as we discuss below, they may not show similar crystal orientations under EBSD.

The mean $\delta^{18}O$ value of DQ grains of the analyzed Ediacara Member samples is 10.58 ± 2.8‰ (1 SD, n=181), and most values are in the range of 8 to 11‰. The mean $\delta^{18}O$ of OQ cements is

18.48 ± 2.5‰ (1 SD, n=298) (Fig. 5). Multiple $\delta^{18}O$ measurements (2–3 analyses using ~11 µm spots) were made within individual quartz overgrowths; the apparent thicknesses of individual overgrowths (as viewed in two-dimensional cross sections) typically range from 8 to 80 µm. In general, early-stage (detrital-grain margin-proximal) OQ cements have higher $\delta^{18}O$ values than later-stage (grain-distal) OQ cements, and characteristically display a pattern of decreasing $\delta^{18}O$ values broadly correlative with distance from the DQ grain margin (Fig. 6, Fig. S11). Significant differences in fossil cement $\delta^{18}O$ values between either disparate fossil taxa or stratigraphic horizons were not observed. The difference between $\delta^{18}O$(OQ) values of the most grain-proximal and most grain-distal cement regions in each individual SIMS transect, which we hereafter describe as "$\Delta^{18}O$(proximal-distal)" was calculated according to the formula $\Delta^{18}O$(proximal-distal) = $\delta^{18}O$(proximal OQ) – $\delta^{18}O$(distal OQ). The majority (91%) of $\Delta^{18}O$(proximal-distal) values of all SIMS analysis transects are positive (Table S1; Fig. S11).

Shapiro-Wilks tests of the $\delta^{18}O$(OQ) data for analyzed samples of the Oscillation-Rippled Sandstone (ORS) Facies and the Planar-Laminated and Rip-Up Sandstone (PLRUS) Facies of the Ediacara Mb. at NENP (in total, n=298) indicate that these data are not normally distributed ($p < 0.05$). Therefore, a Mann-Whitney U test was performed to verify whether these two groups display significant differences in $\delta^{18}O$ values. All tests indicate statistically robust ($p < 0.0001$) significant differences in medians between facies. We observe higher $\delta^{18}O$(OQ) values in the ORS Facies (Fig. 5b, Fig. 5c; Table S2), which has been interpreted to have been deposited in a more proximal environment, and lower values in samples collected from the more distally deposited PLRUS Facies (e.g., Gehling and Droser, 2013; Tarhan et al., 2017; Droser et al., 2022).

We used these SIMS $\delta^{18}O$ data, in conjunction with our petrographic, CL, and EBSD observations, to provide additional constraints on the range of conditions under which the analyzed Ediacara cements precipitated, as discussed in greater detail below.

4. DISCUSSION

4.1 Source of silica

Paired CL, BSE, and SE analyses were used to carefully assess apparent overgrowth-grain relationships and confirm the primary nature of overgrowth zonation.

Limited grain-to-grain contacts or healed fractures indicate that cementation initiated prior to significant compaction and minor occurrences of pressure-solution features such as sutured detrital quartz grain boundaries indicate that the majority of grain-proximal quartz cements did not form during later stages of diagenesis or metamorphism, in agreement with previous studies (e.g., Tarhan et al., 2016) of NENP Ediacara Mb. samples (Fig S1c).

It has been proposed that pressure solution can begin early in the burial history of quartzose sediments (Stone and Siever, 1996), providing a silica source for overgrowth formation. However, the minor intergranular pressure-solution features observed cannot account for the amount of quartz cement observed. These and previous petrographic and geochemical observations, in conjunction with extensive moldic fossilization of a wide range of macroorganisms and organic matgrounds—whose soft-bodied and presumably labile nature would have necessitated relatively rapid fossilization—suggest that the most likely source of the silica from which these earliest cements formed was silica-rich pore fluids in exchange with overlying silica-enriched seawater under fluid-buffered diagenetic conditions (e.g., McBride, 1989; Tarhan et al., 2016; Slagter et al., 2022).

4.2 Electron backscatter diffraction constraints on silica overgrowth mineralogy

Examination of our EBSD data suggests that although quartz overgrowths appear syntaxial (i.e., optically continuous with respect to immediately surrounding detrital quartz grains) when viewed via light microscopy, crystallographic orientations of paired quartz grains and overgrowths within the studied sample areas are not consistently aligned. Paired detrital grains and overgrowths, in some instances, are characterized by similar orientations. However, we noted multiple instances in which orientations appear to be nonuniform as viewed using EBSD (Fig. 4, Figs. S6-S8, Fig. S10). Previous work has highlighted that earlier-forming and less thermodynamically stable silica precipitates, such as amorphous silica and opaline phases, are commonly characterized by a lack of preferred crystallographic orientations or notably more variable orientations (Lynne et al., 2007). During subsequent maturation and transformation to more stable and crystalline phases, authigenic silica precipitates will display increasingly more regular crystallographic orientations. However, later replacive phases will initially pseudomorph and adopt the crystallographic orientation of earlier-forming silica phases (e.g., French and Worden, 2013) and these phase transformations may result in spatially patchy heterogeneity in orientation, even within centimeters, among more crystalline replacive phases such as quartz (Lynne et al., 2007). In this light, the departures from crystallographic alignment we observe via EBSD in some grain-cement pairs may reflect relict heterogeneity related to an amorphous silica precursor.

4.3 Oxygen isotope constraints on overgrowth precipitation conditions

The $\delta^{18}O$ fractionation associated with the precipitation of siliceous phases is strongly temperature-dependent and has therefore been widely used as a proxy for estimating either the temperature of fluids from which silica-rich phases precipitated or the oxygen isotope composition of the precipitating fluid (e.g., Longstaffe and Ayalon, 1991; Pollington et al., 2011). Quartz overgrowths from the Ediacara Mb. show a consistent pattern in which the earliest generations of quartz overgrowths (OQ) (i.e., those cements immediately adjacent to DQ grain boundaries) are characterized by relatively high $\delta^{18}O$ values, and overgrowths are zoned outward, away from grain margins, toward lower $\delta^{18}O$ values (Fig. 6, Fig, S11). This pattern suggests that, in light of the limited pressure solution observed in the Ediacara Mb., temperature and/or fluid $\delta^{18}O$ composition may have varied systematically during ongoing cement precipitation. Increasing temperatures with burial would result in a pattern of higher (lower-temperature) $\delta^{18}O(OQ)$ adjacent to the grains, and lower (higher-temperature) $\delta^{18}O(OQ)$ signatures more distal from the grains. The variability in grain-distal $\delta^{18}O(OQ)$ values between samples further suggests that cement growth ceased at different times for different samples, either when porosity was occluded or upon reaching peak burial conditions (cf., Oye et al., 2020).

In reconstructing a detailed diagenetic history of the Ediacara Mb., a number of parameters, including fluid, stress and thermal history; burial rate; and initial overgrowth silica mineralogy suffer from a paucity of independent constraints. We therefore consider a range of scenarios that could potentially explain observed $\delta^{18}O(OQ)$ patterns in the fossiliferous Ediacara Mb. at NENP. Mean $\delta^{18}O(OQ)$ values in Ediacara Mb. samples (18.48‰) are lower than mean overgrowth $\delta^{18}O$

values previously reported for lower Paleozoic quartzose sandstone-dominated successions of similar age to the Ediacara Mb., such as marine sandstones from the Wisconsin Arch and Illinois Basin of the midwestern USA, including the St. Peter Sandstone (Kelly et al., 2007), Mt. Simon Sandstone (Pollington et al., 2011, 2016; Denny et al., 2017), and Eau Claire Formation (Hyodo et al., 2014). This comparison suggests—under a null set of assumptions that all overgrowths precipitated as quartz, that these cements precipitated concurrently from a single fluid of constant $\delta^{18}O$ composition, and that overgrowths did not experience subsequent alteration—a potentially higher average temperature of precipitation (78–133 °C under the calibration of Sharp et al. 2016; see Table 1) relative to temperatures of cementation proposed for these Cambrian and Ordovician units, which are different in age and diagenetic history (Kelly et al., 2007; Pollington et al., 2011, 2016; Hyodo et al., 2014). Fewer experimental calibration data are available for amorphous silica than for quartz, but calculations performed using the calibration of Kita et al. (1985) yield similar though slightly higher temperature estimates (see Table 1, Table S3, and Supplementary discussion for further discussion of this and other calibrations, including associated uncertainties). However, since $\delta^{18}O$(OQ) is a function of temperature, the isotopic composition of the precipitating fluid, and the history of mineral transformations—each of which, for the Ediacara Mb. at NENP, lack direct, independent empirical constraints—these isotopic data can in theory be explained by several scenarios (e.g., Fig. 7; cf. Hyodo et al., 2014).

The extensive and pre-compactional nature of quartz overgrowths in these samples, without evidence for significant pressure solution, suggests precipitation of at least initial phases occurred under fluid-dominated conditions. In a fluid-dominated system, the $\delta^{18}O$ value of the precipitating fluid ($\delta^{18}O_{fl}$) should not be altered by precipitation of relatively small volumes of cement (Pollington et al., 2011; Fig. S12). If we consider a scenario in which cementation of the Ediacara Mb. occurred under the influence of a mixture of fluids of varying isotopic composition (and potentially over a broader range of timescales), low $\delta^{18}O$ could theoretically also be attributed to meteoric influence, clay mineral dehydration reactions, or later fluid infiltration (Kelly et al., 2007). We consider that leaching by hydrothermal fluids is highly unlikely, due to the lack of evidence of hydrothermal activity in the area (e.g., Tarhan et al., 2016). Additionally, petrographic, SEM, and EPMA data indicate a paucity of clays in these samples (e.g., Fig. 2–4; Tarhan et al., 2016, 2018). We can assess the likelihood of meteoric influence by comparing the two fossiliferous facies analyzed in this study, the ORS Facies—interpreted to have been deposited in a more shoreline-proximal, high-energy and wave-reworked setting—and the PLRUS Facies—inferred to have been deposited in a more offshore setting below wave base (e.g., Gehling and Droser, 2013; Tarhan et al., 2017; Droser et al., 2022). Under a scenario of meteorically influenced OQ $\delta^{18}O$ values, we might expect to see lower $\delta^{18}O(OQ)$ values in the ORS relative to the PLRUS Facies. However, we observe statistically significant (p<0.0001) higher $\delta^{18}O(OQ)$ values in the more shoreline-proximal ORS Facies. Additionally, previous Ge/Si analyses via LA-ICP-MS have indicated no significant differences in Ge/Si values between these facies, nor between these and other fossiliferous Ediacara Mb. facies (Tarhan et al., 2016), further suggesting that long-range fluid transport or two-phase mixing between continentally sourced fluids and seawater provides a less feasible explanation for the source of the precipitating fluids.

On the other hand, if we assume a uniform fluid composition, regardless of its isotopic value, the up to 3.4‰ gradients in $\delta^{18}O(OQ)$ we observe in individual cements (e.g., the approximately 50 μm across which OQ $\delta^{18}O$ values change by this magnitude along a single transect between the analytical loci of LTM9-32-8-O to LTM9-32-13-O; Fig. 4) are consistent with an increase in temperature between the initiation and cessation of cementation during burial (cf. Pollington et al., 2011; Hyodo et al., 2014). Although we cannot directly constrain the burial rate of our analyzed samples because of unknown parameters like burial depth, the $\Delta^{18}O$(proximal–distal OQ) gradients we observe are within the range of previously reported values in Cambrian sandstones (Pollington et al., 2011). However, as discussed below, if phase transformations occurred, any temperature inference gleaned from these isotopic values is likely to reflect a quartz equilibration temperature, rather than the temperature at which an early (and potentially opal-A) precursor silica phase formed.

The $\delta^{18}O$ value of the precipitating fluid(s) represents another source of uncertainty; for instance, a wide range of $\delta^{18}O$ values have been suggested for Proterozoic and early Paleozoic seawater, from −3‰ (marine carbonate isotope data; Came et al., 2007; Jaffrés et al., 2007) to −1‰ (carbonate clumped isotope data; Bergmann et al., 2018), +1‰ (chert triple oxygen isotope data; Sengupta et al., 2020) or ca. −5 to −9‰ (iron oxide oxygen isotope data and thermal modeling; Galili et al., 2019; Guo et al., 2022; Tatzel et al., 2022). These $\delta^{18}O_{fl}$ estimates in turn yield highly variable, moderate to elevated estimated average temperatures of precipitation for Ediacara Mb. overgrowths (Table 1; Fig. 7; see Supplementary material for calculations and additional discussion). In sum, under assumptions of a relatively high and constant $\delta^{18}O_{fl}$ value, the temperatures we calculate are unlikely to be feasible for seawater-derived fluids, suggesting either that quartz overgrowths formed later in the burial history of the Ediacara Mb., that a lower fluid isotopic composition may provide a more parsimonious explanation for these data, or that original values were reset during diagenesis (for instance, during silica phase transformations; see section 4.4, below).

Our EBSD and CL data do not support a scenario of late-stage overgrowth initiation; our petrographic observations (see above) indicate a relatively early diagenetic initiation of cementation. Moreover, the consistent zonation we observe in both overgrowth morphology and $\delta^{18}O$(OQ), from higher grain-proximal $\delta^{18}O$ values to lower grain-distal $\delta^{18}O$ values, also indicate preservation of a signal of early-initiating and progressive silica cementation. Moreover, these observations also dovetail with several previous studies that posit that quartz cementation may begin below 70–80 °C (Kraishan et al., 2000; Marchand et al., 2002; Kelly et al., 2007; Pollington et al., 2011). This bolsters previous assertions that silica for early-forming quartz cements might, in some cases, have been sourced from seawater or early diagenetic porewaters (Harwood et al., 2013). This interpretation supports recent hypotheses for the role of early-diagenetic silica cementation in facilitating extensive Ediacara-style moldic fossilization of a wide range of soft-bodied macroorganisms and organic matgrounds (Tarhan et al., 2016; Slagter et al., 2021, 2022). An early onset of silica cementation would have played a critical role in stabilizing surrounding sands sufficiently rapidly to capture detailed morphological impressions of buried seafloor communities prior to extensive decay.

4.4 Silica diagenesis

Experimental data indicate that precipitation of quartz at low temperatures is dominated by kinetic processes (Pollington et al., 2016; Fernandez et al., 2019), and its growth rate is a logarithmic function of temperature, assuming linear growth from grain boundaries according to

Walderhaug's (1996) model. The majority of our samples display a trend of positive $\Delta^{18}O$(proximal-distal) values, with more grain-proximal cements characterized by higher $\delta^{18}O$ values and more distal cements characterized by lower $\delta^{18}O$ values (Table S1). However, $\delta^{18}O$ values may also reflect the impact of diagenesis (Liljestrand et al., 2021; Tatzel et al., 2022); the calculated temperatures described above may record the transition from opal-A to quartz, rather than the temperature of initial precipitation (cf. Ibarra et al., 2022). The fact that we observe well-preserved CL zonation and associated $\delta^{18}O$ trends indicates that either (i) overgrowths were initially precipitated as an amorphous phase (opal-A) and later transformed to quartz by stages, preserving zoned textures; (ii) those overgrowths most proximal to quartz grains were initially precipitated as an amorphous phase, and later overgrowth stages were subsequently precipitated under moderate to higher temperatures as quartz, thereby preserving zoned textures, or (iii) all overgrowth stages were precipitated as quartz, and faithfully represent initial precipitation conditions (Fig. 7). Scenarios (i) and (ii) are supported by EBSD data indicating a lack of consistent crystallographic alignment between detrital quartz grains and adjacent quartz overgrowths (Fig. 4, Figs. S6-10).

In addition, experimental data suggest that cements are likely to have initially precipitated as amorphous silica phases through complexation with shallowly buried macrofossil and matground organics. Complexation of dissolved silica with silica-reactive organic functional groups in organism tissues may have facilitated amorphous silica precipitation even from undersaturated fluids (cf. Slagter et al., 2021). In this scenario, precipitated silica cements may have subsequently undergone transformations of opal-A$\rightarrow$ quartz (potentially via an opal-CT intermediary stage; cf. Kastner et al., 1977). During these phase transitions, silica oxygen isotopic signatures may have experienced exchange and re-equilibration with local pore fluids (cf. Trower et al., 2021; Yanchilina et al., 2021). Opal-A(-opal-CT)-quartz transformations tend to occur over relatively narrow temperature windows (Varkouhi et al., 2021). Thus, it is possible that the mineralogical transition of an amorphous silica phase to crystalline α-quartz through Ostwald ripening, i.e., dissolution and reprecipitation into more stable phases (Iler, 1979), happened relatively early in the burial history of the Ediacara Mb., under moderate temperatures, albeit elevated relative to typical surface conditions (e.g., 21–99 °C, depending on calibration scheme and initial $\delta^{18}O_{fluid}$ composition; Table 1). Scenario (iii) is supported by previous research suggesting that quartz can precipitate under lower temperatures than previously appreciated (e.g., 10−30 °C; e.g., Kelly et al., 2007) in the absence of other phases such as chalcedony or opaline silica. In light of petrographic and CL evidence for zonation and limited pressure solution; EBSD evidence for inconsistent crystallographic alignment between DQ and OQ; consistently zoned but moderate $\delta^{18}O$(OQ) values; and the close association between overgrowths and what would have been high concentrations of benthic organic matter, as inferred from the abundant and dense macrofossil and TOS assemblages preserved at NENP and in these samples, we consider scenario (ii) to offer the most plausible explanation for Ediacara Mb. overgrowths. Additional independent constraints on the burial history and authigenic silica phase evolution of Ediacaran strata at NENP will in future, we hope, provide further insights into the original mineralogy (i.e., silica phase) of Ediacara Mb. silica overgrowths.

Some previous studies have interpreted quartz cementation as an episodic process (e.g., Marchand et al., 2002) whereas others (e.g., Walderhaug, 1996) have favored a model of continuous quartz growth with increasing temperatures and quartz surface area during burial.

Considering the pattern we observe of higher $\delta^{18}O(OQ)$ values adjacent to detrital quartz grain boundaries and decreasing to lower $\delta^{18}O(OQ)$ values further from the grains, we consider that the earliest OQ cements (most proximal to DQ grain boundaries) in the analyzed Ediacara Mb. samples likely record precipitation under lower temperatures, and that subsequent generations of overgrowths were precipitated as quartz under increasing temperatures during burial diagenesis. The earliest (most grain-proximal) cements are characterized by clear zonation (Fig. 3b), which may support an episodic and relatively rapid process, whereas cements located more distally from grain margins may potentially reflect a secondary, longer, and continuous process. This interpretation agrees with previous paleontological, geological (Tarhan et al., 2016), and experimental (Slagter et al., 2021) data that indicate that the most grain-proximal generations of silica cements formed early in the burial history of the Ediacara Mb., facilitating the formation of casts and molds of the soft-bodied Ediacara Biota, and that this early stage of silicification was subsequently followed by later continuous or episodic silica cementation.

5. CONCLUSIONS

In situ SIMS oxygen isotope analyses, combined with BSE, CL, and EBSD imaging, provide unique spatial insights into the relationship between quartz grains and overgrowths and elucidate the thermal and fluid history of cementation in the Ediacara Mb.—a unit that hosts some of the richest Ediacara Biota fossil assemblages worldwide and provides a critical window into early animal evolution. Fossiliferous samples from the Ediacara Mb. contain clear generations of quartz overgrowths precipitated concentrically on detrital quartz grains. Likewise, the zoning we observe in $\delta^{18}O(OQ)$ values, with characteristically positive $\Delta^{18}O$ (proximal–distal OQ) values, most parsimoniously indicates growth under increasing temperatures. Textural, mineralogical, and $\delta^{18}O$ data assessed across grain-cement transects indicate an early diagenetic origin for the most grain-proximal cements. Measured $\delta^{18}O$ values likely indicate the relatively low temperatures at which phase transformations between opaline silica and quartz may have occurred during recrystallization, followed by continued quartz cementation under higher-temperature burial conditions. These trends represent continued, though possibly punctuated, cement growth during the potentially long-ranging diagenetic history of this unit. These data corroborate previous proposals that early silica cementation played a key role in the moldic fossilization of the Ediacara Biota and indicate that cementation was not confined to early diagenesis but continued through substantially later stages in the burial history of the Ediacara Member.

6. ACKNOWLEDGEMENTS

This research was supported by the NASA Exobiology program (grant 80NSSC19K0472 to L.G.T. and M.L.D.). We thank Z. Jiang and B. Schneider for assistance with SEM-EDS, SEM-CL, and SEM-EBSD imaging; J. Eckert for assistance with EMP-CL analyses; and M. Spicuzza for assistance with SIMS sample preparation. We are grateful to Ross and Jane Fargher for facilitating access to Nilpena Ediacara National Park, acknowledging that this land lies within the Adnyamathanha Traditional Lands. We thank N. Planavsky, J. Wang, M. Brandon, and J. Gehling for discussion. WiscSIMS is supported by NSF (EAR-2004618) and the University of Wisconsin-Madison.

REFERENCES

Bergmann, K.D., Al Balushi, S.A., MacKey, T.J., Grotzinger, J.P., Eiler, J.M., 2018. A 600-million-year carbonate clumped-isotope record from the Sultanate of Oman. J. Sediment. Res. 88, 960–979.

Bobrovskiy, I., Krasnova, A. Ivantsov, A., Serezhnikova, E.L., Brocks J.J. 2019. Simple sediment rheology explains the Ediacara biota preservation. Nat. Ecol. and Evol., 3, 582–598.

Butterfield, N. J., 2003, Exceptional fossil preservation and the Cambrian explosion: Integrative and Comparative Biology, 43, 166-177.

Came, R.E., Eiler, J.M., Veizer, J., Azmy, K., Brand, U., Weidman, C.R., 2007. Coupling of surface temperatures and atmospheric CO2 concentrations during the Palaeozoic Era. Nature 449, 198–201.

Cavosie, A.J., Valley, J.W., Wilde, S.A., E.I.M.F., 2005. Magmatic $\delta^{18}O$ in 4400–3900 Ma detrital zircons: a record of the alteration and recycling of crust in the Early Archean. Earth Planet. Sci. Lett. 235, 663–681.

Clayton, R.N., Mayeda, T.K., O'Neil, J. R., 1972. Oxygen isotope exchange between quartz and water. J. Geophys. Res. 77, 3057–3067.

Denny, A.C., Kozdon R., Kitajima, K., Valley, J. W., 2017. Isotopically zoned carbonate cements in Early Paleozoic sandstones of the Illinois Basin: $\delta^{18}O$ and $\delta^{13}C$ records of burial and fluid flow. Sed. Geol., 361, 93-110.

Dickson, J.A.D. 2023. Insights into the growth morphology of calcite cement. The Depositional Record, 9, 457–481.

Droser, M.L., Tarhan, L. G., Gehling, J.G., 2017. The rise of animals in a changing environment: global ecological innovation in the late Ediacaran. Annu. Rev. Earth Planet. Sci. 45, 593–617.

Droser, M. L., *et al.* 2019. Piecing together the puzzle of the Ediacara Biota: Excavation and reconstruction at the Ediacara National Heritage site Nilpena (South Australia). Palaeogeogr. Palaeoclimatol. Palaeoecol. 513, 132-145.

Droser, M.L., Tarhan, L.G., Evans, S. D., Surprenant, R.L., Gehling, J.G., 2020. Biostratinomy of the Ediacara Member (Rawnsley Quartzite, South Australia): implications for depositional environments, ecology and biology of Ediacara organisms. Interface Focus 10 (4), 20190100.

Droser, M.L., Evans, S.D., Tarhan, L.G., Surprenant, R.L., Hughes, I.V., Hughes, E.B., Gehling, J.G., 2022. What Happens Between Depositional Events, Stays Between Depositional Events: The Significance of Organic Mat Surfaces in the Capture of Ediacara Communities and the Sedimentary Rocks That Preserve Them. Frontiers in Earth Science 10, 826353.

Dong, L., et al. 2015. Germanium/silicon of the Ediacaran-Cambrian Laobao cherts: Implications for the bedded chert formation and paleoenvironment interpretations. Geochem. Geophys. Geosyst., 16, 751–763.

Fernandez, N.M., Zhang, X., Druhan, J.L., 2019. Silicon isotopic re-equilibration during amorphous silica precipitation and implications for isotopic signatures in geochemical proxies. Geochim. Cosmochim. Acta 262, 104-127.

French, M.W., Worden, R.H., 2013. Orientation of microcrystalline quartz in the Fountainebleau Formation, Paris Basin and why it preserves porosity. Sed. Geol. 284–285, 149–158.

Galili, N., Shemesh, A., Yam, R., Brailovsky, I., Sela-Adler, M., Schuster, E.M., Collom, C., Bekker, A., Planavsky, N., Macdonald, F.A., Préat, A., Rudmin, M., Trela, W., Sturesson, U., Heikoop, J.M., Aurell, M., Ramajo, J., Halevy, I., 2019. The geologic history of seawater oxygen isotopes from marine iron oxides. Science 365 (6452), 469-473.

Gehling, J. G. 1999. Microbial mats in terminal Proterozoic siliciclastics: Ediacaran death masks. Palaios, 14, 40–57.

Gehling, J.G., Droser, M.L., 2013. How well do fossil assemblages of the Ediacara Biota tell time? Geology 41, 447–450.

Gehling, J.G., 2000. Environmental interpretation and a sequence stratigraphic framework for the terminal Proterozoic Ediacara Member within the Rawnsley Quartzite, South Australia. Precambr. Res. 100, 65–95.

Guo, M., Wostbrock, J.A. G., Planavsky N.J., Korenaga J., 2022. Reconstructing seawater $\delta^{18}O$ and system evolution O values with solid Earth. Earth Planet. Sci. Lett. 592, 117637.

Harwood, J., Aplin, A.C., Fialips, C.I., Iliffe, J.E., Kozdon, R., Ushikubo, T., Valley, J.W., 2013. Quartz cementation history of sandstones revealed by high-resolution SIMS oxygen isotope analysis. J. Sediment. Res. 83, 522–530.

Heck, P.R., Huberty, J. M., Kita, N.T., Ushikubo, T., Kozdon, R., Valley, J.W., 2011. SIMS analyses of silicon and oxygen isotope ratios for quartz from Archean and Paleoproterozoic banded iron formations. Geochim. Cosmochim. Acta 75, 20, 5879-5891.

Hyodo, A., Kozdon, R., Pollington, A.D., Valley, J.W., 2014. Evolution of quartz cementation and burial history of the Eau Claire Formation based on in situ oxygen isotope analysis of quartz overgrowths. Chem. Geol. 384, 168–180.

Ibarra, D.E., Yanchilina, A.G., Lloyd, M. K., Methner, K.A., Chamberlain, C.P., Yam, R., Shemesh, A., Stolper, D.A., 2022. Triple oxygen isotope systematics of diagenetic recrystallization of diatom opal-A to opal-CT to microquartz in deep sea sediments. Geochim. Cosmochim. Acta 320, 304–323.

Iler, K.R., 1979. The Chemistry of Silica: Solubility, Polymerization, Colloid and Surface Properties, and Biochemistry. John Wiley & Sons, New York.

Jaffrés, J.B.D., Shields, G.A., Wallmann, K., 2007. The oxygen isotope evolution of seawater: A critical review of a long-standing controversy and an improved geological water cycle model for the past 3.4 billion years. Earth Sci. Rev. 83, 83–122.

Kastner, M., Keene, J.B., Gieskes, J.M., 1977. Diagenesis of siliceous oozes – I. Chemical controls on the rate of opal-A to opal-CT transformation – an experimental study. Geochim. Cosmochim. Acta 41 (8), 1041–1051.

Kelly, J.L., Fu, B., Kita, N.T., Valley, J.W., 2007. Optically continuous silcrete quartz cements of the St. Peter Sandstone: high precision oxygen isotope analysis by ion microprobe. Geochim. Cosmochim. Acta 71 (15), 3812–3832.

Kidder. L., Tomescu, I., 2016. Biogenic chert and the Ordovician silica cycle. Palaeogeogr. Palaeoclimatol. Palaeoecol. 458, 29-38,

Kita, N., Ushikubo, T., Fu, B., Valley, J.W., 2009. High Precision SIMS oxygen isotope analysis and the effect of sample topography. Chem. Geol. 264, 43-57.

Kita, I., Taguchi, S., Matsubaya, O. 1985. Oxygen isotope fractionation between amorphous silica and water at 34–93°C. Nature 314, 83–84.

Kraishan, G.M., Rezaee, M.R., Worden, R.H., 2000. Significance of trace element composition of quartz cement as a key to reveal the origin of silica in sandstones: an example from the Cretaceous of the Barrow Sub-Basin, Western Australia, in Worden, R.H., and Morad, S., eds., Quartz Cementation in Sandstones: International Association of Sedimentologists, Special Publication 29, 317–331.

Laflamme, M., Schiffbauer, J. D., Narbonne, G. M., & Briggs, D. E. G. 2011. Microbial biofilms and the preservation of the Ediacara biota. Lethaia*, 44,* 203–213.

Liljestrand, F., Hania A., Giordano, M., Johnston, D., 2021. Calibrating the triple oxygen isotope signature of cultured diatoms. Limnology and Oceanography 66(12), 4254–4266.

Linzmeier, B.J., Kitajima, K., Denny, A. C., Cammack, J.N., 2018. Making maps on a micrometer scale, Eos, 99.

Lloyd, J.C., Blades, M.L., Counts, J.W., Collins, A.S., Amos, K.J., Wade, B.P., Hall, J.W., Hore, S., Ball, A.L., Shahin, S. and Drabsch, M., 2020. Neoproterozoic geochronology and provenance of the Adelaide Superbasin. Precambr. Res. 350, 105849.

Longstaffe, F.J., Ayalon, A., 1991. Mineralogical and O-isotope studies of diagenesis and porewater evolution in continental sandstones, Cretaceous Belly River Group, Alberta, Canada. Appl. Geochem. 6 (3), 291-303.

Lynne, B.Y., Campbell, K.A., James, B.J., Browne, P.R.L., Moore, J., 2007. Tracking crystallinity in siliceous hot-spring deposits. Amer. Jour. Sci. 307, 612–641.

MacGabhann, B.A., Schiffbauer, J.D., Hagadorn, J. W., Van Roy, P., Lynch, E. P., Morrison, L., Murray, J. 2019. Resolution of the earliest metazoan record: Differential taphonomy of Ediacaran and Paleozoic fossil molds and casts. Palaeogeogr. Palaeoclimatol. Palaeoecol, 513,146-165.

Marchand, A.M.E., MaCaulay, C.I., Haszeldine, R.S., Fallick, A.E., 2002. Pore water evolution in oilfield sandstones: constraints from oxygen isotope microanalyses of quartz cement. Chem. Geol. 191, 285–304.

McBride, E.F., 1989. Quartz cement in sandstones: a review: Earth Sci. Rev. 26, 69–112.

Narbonne, G.M., 2005. The Ediacara Biota: Neoproterozoic Origin of Animals and Their Ecosystems. Ann. Rev. Earth and Planet. Sci. 33, 421–442.

Oye, O.J., Aplin, A.C., Jones, S.J., Gluyas, J.G., Bowen, L., Harwood, J., Orland, I.J., Valley, J.W., 2020. Vertical effective stress and temperature as controls of quartz cementation in sandstones: evidence from North Sea Fulmar and Gulf of Mexico Wilcox sandstones. Mar. Petrol. Geol. 115, 104289.

Paterson, J.R., Gehling, J.G., Droser, M.L., Bicknell, R.D.C., 2017. Rheotaxis in the Ediacaran epibenthic organism *Parvancorina* from South Australia. Sci. Rep. 7, 45539.

Pittman, E. D., 1979, Porosity, diagenesis and productive capability of sandstone reservoirs, *in* Scholle, P. A., and Schluger, P. R., eds., Aspects of Diagenesis: Tulsa, Oklahoma, Society of Economic Paleontologists and Mineralogists, 159-173.

Pollington, A.D., Kozdon, R., Valley, J.W., 2011. Evolution of quartz cementation during burial of the Cambrian Mount Simon Sandstone, Illinois Basin: in situ microanalysis of $\delta^{18}O$. Geology, 39 (12), 1119–1122.

Pollington, A.D., Kozdon, R., Anovitz, L.M., Georg, R.B., Spicuzza, M.J., Valley, J.W., 2016. Experimental calibration of silicon and oxygen isotope fractionation between quartz and water at 250 °C by in situ microanalysis of experimental products and application to natural samples. Chem. Geol. 421, 127–142.

Ramseyer, K., et al., 2013. Primary silica precipitate at the Precambrian/Cambrian boundary in the South Oman Salt Basin, Sultanate of Oman. Mar. Pet. Geol. 39, 187–197.

Reid L.M., Payne J.L., García-Bellido D.C., Jago J.B., 2020. The Ediacara Member, South Australia: lithofacies and palaeoenvironments of the Ediacara biota. Gondwana Res. 80, 321–334.

Sibley, D.F., Blatt, H., 1976. Intergranular pressure solution and cementation of the Tuscarora orthoquartzite. J. Sediment. Res. 46, 881–896.

Sengupta, S. Peters, S.T.M., Reitner, J., Duda J.P., Pack, A., 2020. Triple oxygen isotopes of cherts through time. Chem. Geol. 3554, 119789.

Siever, R. 1992. The silica cycle in the Precambrian. Geochim. et Cosmochim. Acta, 56, 3265–3272.

Slagter, S., Tarhan, L.G., Hao, W, Planavsky, N.J., Konhauser, K.O., 2021. Experimental evidence supports early silica cementation of the Ediacara Biota. Geology 49, 51–55.

Slagter, S., Hao, W., Planavsky, N.J., Konhauser, K.O., Tarhan, L.G., 2022. Biofilms as agents of Ediacara-style fossilization. Sci. Rep. 12, 8631.

Stone, W.N., Siever, R., 1996. Quantifying compaction, pressure solution and quartz cementation in moderately- and deeply-buried quartzose sandstones from the Greater Green River Basin, Wyoming, in Crossey, L.J., et al., eds., Siliciclastic diagenesis and fluid flow: Concepts and applications: SEPM (Society for Sedimentary Geology) Special Publication 55, 129–150.

Surprenant, R.L., Gehling, J.G., Droser, M.L., 2020. Biological and Ecological Insights from the Preservational Variability of *Funisia Dorothea*, Ediacara Member, South Australia. Palaios 35, 359–376.

Tarhan L.G., Droser, M.L., Gehling, J.G., 2015. Depositional and preservational environments of the Ediacara Member, Rawnsley Quartzite (South Australia): Assessment of paleoenvironmental proxies and the timing of 'ferruginization'. Palaeogeogr. Palaeoclimatol. Palaeoecol. 434, 4-13

Tarhan, L.G., Hood, A.v.S., Droser, M.L., Gehling, J.G., Briggs, D.E.G., 2016. Exceptional preservation of soft-bodied Ediacara Biota promoted by silica-rich oceans. Geology 44, 951–954.

Tarhan, L.G., Droser, M.L., Gehling, J.G., Dzaugis, M.P., 2017. Microbial mat sandwiches and other anactualistic sedimentary features of the Ediacara Member (Rawnsley Quartzite, South Australia): Implications for interpretation of the Ediacaran sedimentary record. Palaios 32, 181–194.

Tarhan, L.G., Droser, M.L., Gehling, J.G., 2022. Picking out the warp and weft of the Ediacaran seafloor: Paleoenvironment and paleoecology of an Ediacara textured organic surface. Precambr. Res. 369, 106539.

Tarhan, L.G., Planavsky, N.J., Wang, X., Bellefroid, E.J., Droser, M.L. and Gehling, J.G., 2018. Late-stage 'ferruginization' of the Ediacara Member (Rawnsley Quartzite, South Australia): insights from uranium isotopes. Geobiology 16, 35–48.

Tatzel, M., Frings, P.J., Oelze, M., Herwartz, D., Lünsdorf, N. K., Weidenbeck, M., 2022. Chert oxygen isotope ratios are driven by Earth's thermal evolution. PNAS 119 (51) e2213076119.

Trower, E.J., Strauss, J.V., Sperling, E.A., Fischer, W.W., 2021. Isotopic analyses of Ordovician–Silurian siliceous skeletons indicate silica-depleted Paleozoic oceans. Geobiology 19, 460–472.

Varkouhi, S., Tosca N. J., Cartwright J. A., 2021. Temperature–time relationships and their implications for thermal history and modelling of silica diagenesis in deep-sea sediments. Mar. Geol. 439, 106541.

Valley, J.W. and Kita, N.T., 2009. In situ oxygen isotope geochemistry by ion microprobe. MAC Short Course: Secondary Ion Mass Spectrometry in the Earth Sciences 41, 19–63.

Wade, M. 1968. Preservation of soft-bodied animals in Precambrian sandstones at Ediacara, South Australia. Lethaia, 1, 238–267.

Walderhaug, O., 1996. Kinetic modeling of quartz cementation and porosity loss in deeply buried sandstone reservoirs. American Association of Petroleum Geologists Bulletin 80, 731–745.

Wang, X.L., Coble, M.A., Valley, J.W., Shu, X.J., Kitajima, K., Spicuzza, M.J., Sun, T., 2014. Influence of radiation damage on Late Jurassic zircon from southern China: evidence from in situ measurements of oxygen isotopes, laser Raman, U-Pb ages, and trace elements. Chem. Geol. 389, 122–136.

Yanchilina, A.G., Yam, R., Shemesh, A., 2021. The effect of sediment lithology on oxygen isotope composition and phase transformation of marine biogenic opal. Chem. Geol. 570, 120-175.

FIGURE CAPTIONS

Figure 1. Ediacara fossils in sample (a) MAB-A showing *Aspidella*, indicated by white arrows, associated with sandstone-hosted sandstone intraclasts (cf. Tarhan et al., 2017), examples denoted by yellow arrows; and (b) Eo-2 showing *Eoandromeda*, indicated by a white arrow,

associated with textured organic surfaces comprised of dense aggregations of the tubular macrofossil *Plexus*, example denoted by a yellow arrow. See Table S1 and references therein for further locality, facies, bedding-plane and fossil assemblage information.

Figure 2. Photomicrographs of samples (a) STC-2 and (b) TC-MM3-2 showing detrital quartz (DQ) and overgrowth quartz (OQ), with labeled examples. See Table S1 and references therein for further locality, facies, bedding-plane and fossil assemblage information. Images taken under cross-polarized light.

Figure 3. Scanning electron microscope cathodoluminescence images of detrital quartz (DQ) and overgrowth quartz (OQ) associated with sample areas (a) LTM12-78; and (b) LTM9-84 from the Ediacara Mb., with examples of concentric OQ indicated by arrows. Inset with dashed lines indicates overgrowth zonation representing discrete stages of precipitation.

Figure 4. (a) EBSD orientation image of sample area LTM9-32 overlain on a BSE image, with a step size of 2 μm, showing that quartz overgrowths are not uniformly in the same optical orientation as detrital quartz grains. White dots indicate the locations of SIMS analyses. Crystal orientation parallel to the sample Z direction (an inverse pole figure Z map) is shown by the color legend in the inset figure. (b) SEM-CL image of the same area, taken following SIMS analyses and showing labeled examples of detrital quartz grains (DQ) and overgrowths (OQ). (c) SEM-CL image of quartz grains and overgrowths overlain by associated SIMS $\delta^{18}O$ data, reported with respect to VSMOW—Vienna Standard Mean Ocean Water. (d) Backscattered electron (BSE) image showing the location of SIMS analysis pits.

Figure 5. Histograms of oxygen isotope ratios from the Ediacara Mb., measured *in situ* from detrital quartz grains (DQ) and overgrowths (OQ) for (a) all data, (b) the ORS Facies, and (c) the PLRUS Facies. Mann-Whitney U test results indicate significantly higher $\delta^{18}O$ (OQ) values in the ORS Facies than in the PLRUS Facies ($p<0.0001$). Note different vertical scales in each graph. All values are reported with respect to VSMOW—Vienna Standard Mean Ocean Water.

Figure 6. SIMS $\delta^{18}O$ analyses measured along transects from detrital quartz (DQ) to overgrowth quartz (OQ), overlain on false-color EPMA-CL images for sample areas (a) LTM7-4, and (b) LTM8-9 from the Ediacara Mb. All values are reported with respect to VSMOW—Vienna Standard Mean Ocean Water. Oxygen isotope ratios measured over traverse a-a', and b-b' overgrowths (OQ) are projected in (c) LTM7-4, and (d) LTM8-9. Distance is calculated from the center of each OQ ablation pit to the boundary of the associated detrital grain (a and b, respectively). Error bars (2SD) are smaller than the size of the symbols. Data show an overall decrease in $\delta^{18}O$ (OQ) with distance away from the detrital quartz (DQ) grain boundary.

Figure 7. (a) Temperature calculations for maximum, mean, and minimum $\delta^{18}O$(OQ) values observed in the analyzed SIMS dataset under different calibration schemes. (b) Schematic of potential diagenetic scenarios that could explain OQ $\delta^{18}O$ observations from the Ediacara Member. Plot of $\delta^{18}O_{fl}$ in equilibrium with quartz cement (OQ) $\delta^{18}O$ values. The contours indicate calculations under the null assumption that quartz cements precipitated in equilibrium with precipitating fluids (pure H_2O, Sharp et al., 2016), as a function of temperature for the maximum, 26.7 ‰; mean, 18.48 ‰; and minimum, 7.5‰ $\delta^{18}O$(OQ) values observed in the

analyzed SIMS dataset. Arrows with numbers indicate four potential (non-exhaustive) end-member scenarios for the evolution of precipitating fluid $\delta^{18}O$ composition and temperature: [1] constant high temperature and variable fluid $\delta^{18}O$ ($\delta^{18}O_{fl}$); [2] constant lower temperature and variable $\delta^{18}O_{fl}$; [3] variable temperature and constant higher $\delta^{18}O_{fl}$ (seawater, following Jaffrés et al., 2007 after a compilation of marine carbonate data); and [4] variable temperature and constant lower $\delta^{18}O_{fl}$, (following Galili et al., 2019; Guo et al., 2022; Tatzel et al., 2022, as indicated by iron oxide and chert data). Available petrographic, EBSD, and SIMS $\delta^{18}O$ data indicate that scenario 4 may provide, of the four scenarios described in this plot, the most parsimonious explanation for the silica cementation of Ediacara Mb. fossiliferous samples analyzed in this study, with $\delta^{18}O$ values of earlier-forming overgrowths reflecting temperatures of re-precipitation during fluid-buffered early-diagenetic phase transformations from amorphous silica to quartz. Figure modified from Hyodo et al. (2014).


a
0 5 10 mm
b
0 5 10 mm

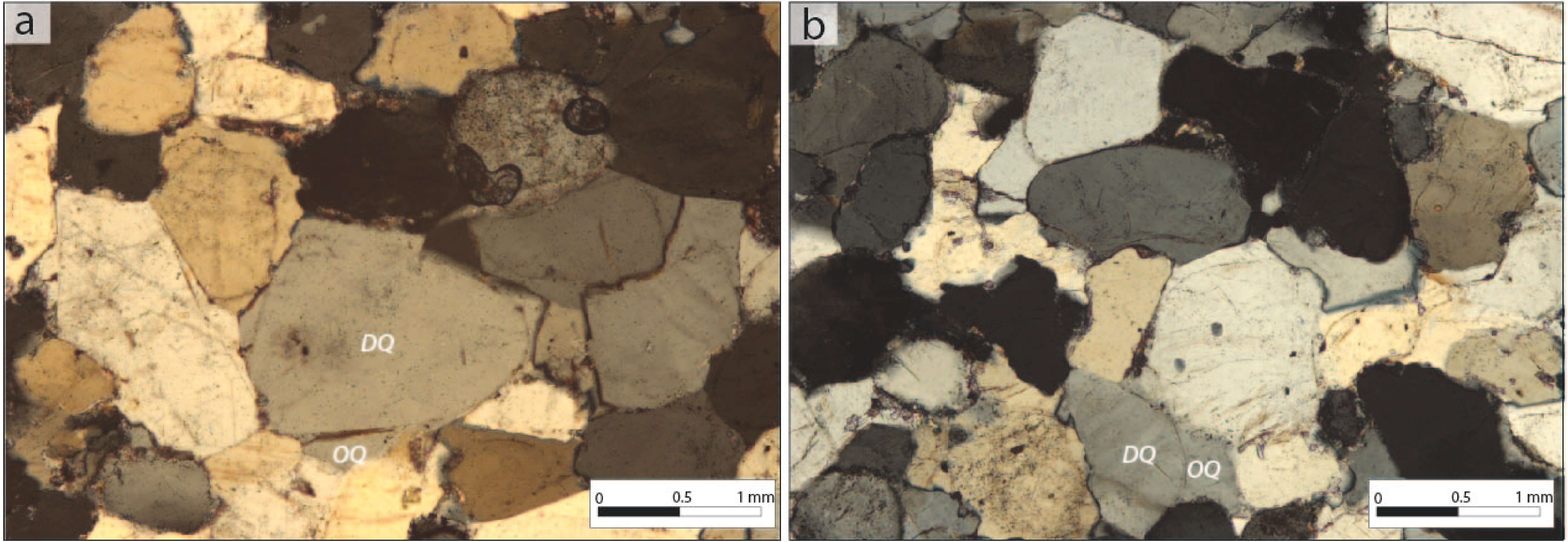
a
DQ
OQ
0
0.5
1 mm
b
DQ
OQ
0
0.5
1 mm

a
0
25
50 µm
DQ
OQ
b
0
25
50 µm
DQ
OQ

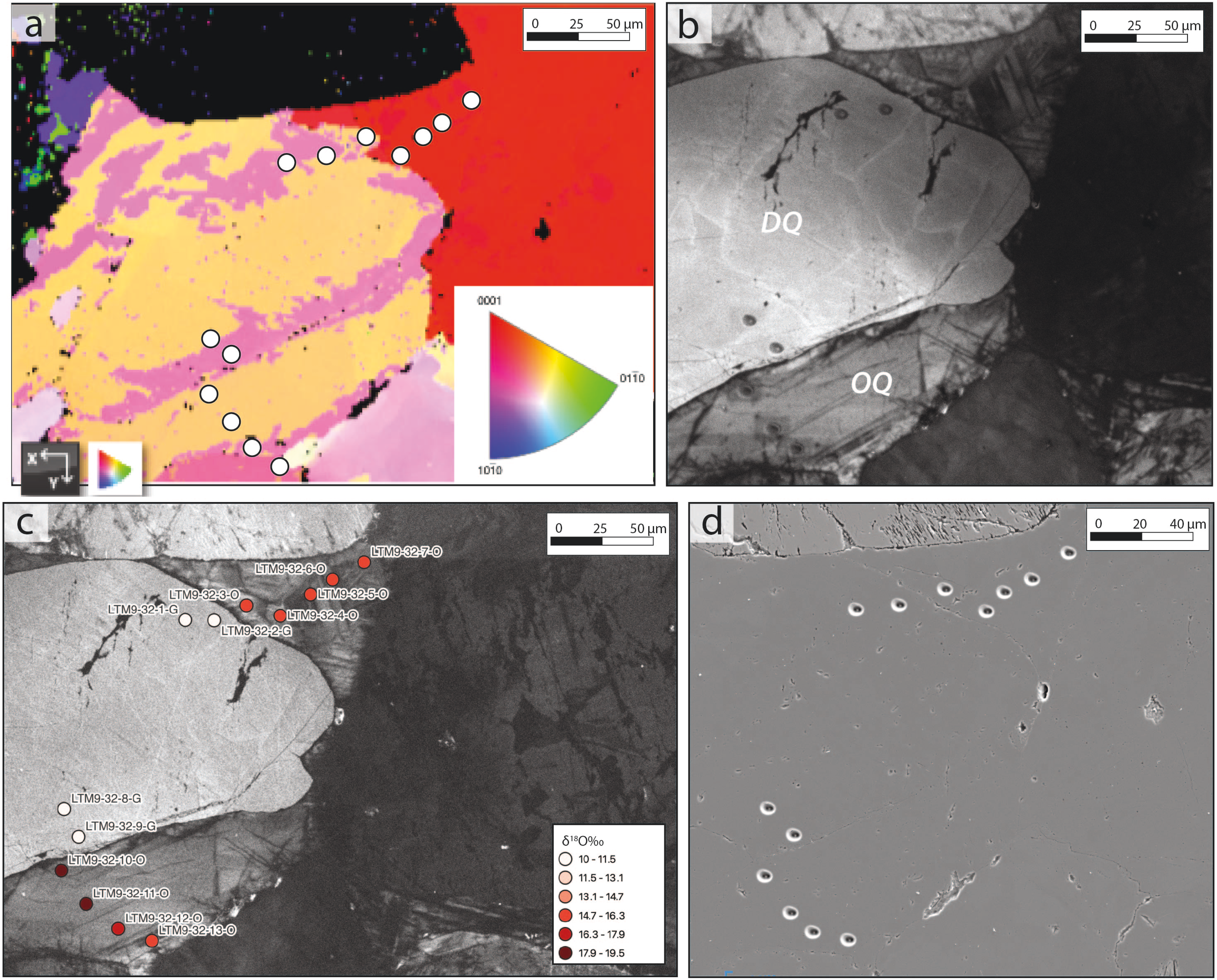

a
0 25 50 µm
0001
01$\bar{1}$0
10$\bar{1}$0
x
y
b
0 25 50 µm
DQ
OQ
c
0 25 50 µm
LTM9-32-7-O
LTM9-32-6-O
LTM9-32-3-O
LTM9-32-5-O
LTM9-32-1-G
LTM9-32-4-O
LTM9-32-2-G
LTM9-32-8-G
LTM9-32-9-G
LTM9-32-10-O
LTM9-32-11-O
LTM9-32-12-O
LTM9-32-13-O
δ18O‰
10 - 11.5
11.5 - 13.1
13.1 - 14.7
14.7 - 16.3
16.3 - 17.9
17.9 - 19.5
d
0 20 40 µm

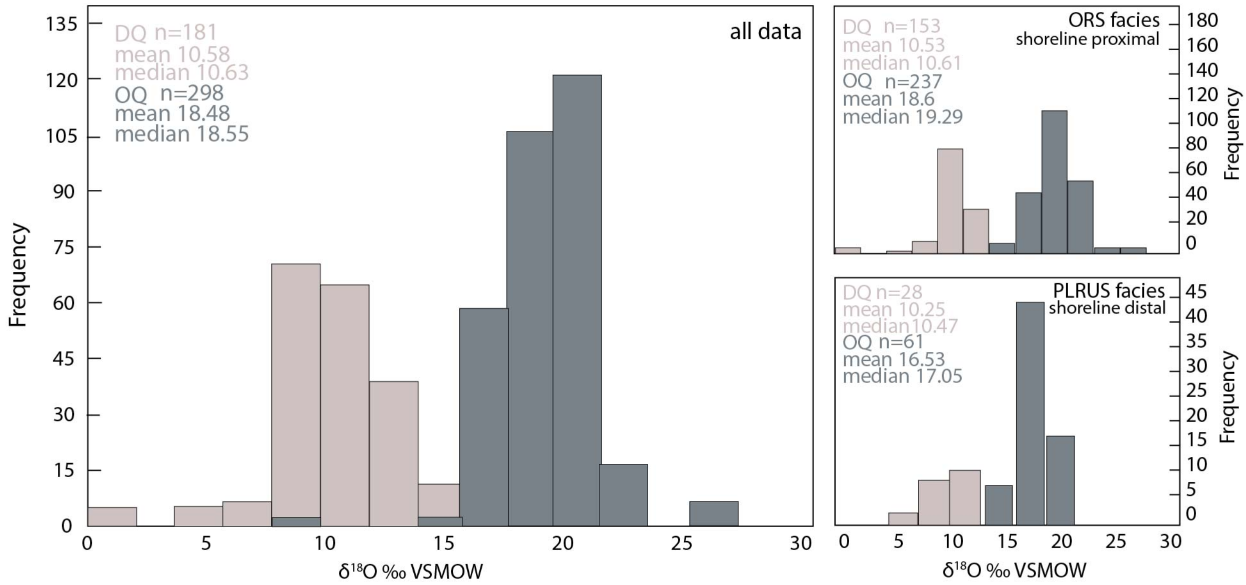

all data
DQ n=181
mean 10.58
median 10.63
OQ n=298
mean 18.48
median 18.55
Frequency
0
15
30
45
60
75
90
105
120
135
0
5
10
15
20
25
30
δ18O ‰ VSMOW
ORS facies
shoreline proximal
DQ n=153
mean 10.53
median 10.61
OQ n=237
mean 18.6
median 19.29
0
20
40
60
80
100
120
140
160
180
Frequency
PLRUS facies
shoreline distal
DQ n=28
mean 10.25
median10.47
OQ n=61
mean 16.53
median 17.05
0
5
10
15
20
25
30
35
40
45
Frequency
0
5
10
15
20
25
30
δ18O ‰ VSMOW


a
b
a
a′
LTM7-4-20-G
LTM7-4-19b-O
LTM7-4-19-O
LTM7-4-18-O
LTM7-4-17-O
LTM7-4-16-G
δ18O‰
0.1 - 3.6
3.6 - 7
7 - 10.4
10.4 - 13.9
13.9 - 17.3
17.3 - 20.7
0 25 50 µm
LTM8-9-8-G
LTM8-9-10-O
LTM8-9-9-O
LTM8-9-11-O
LTM8-9-13-G
LTM8-9-12-G
b′
LTM8-9-23-G
LTM8-9-22-O
LTM8-9-21-O
LTM8-9-20-O
LTM8-9-18-O
LTM8-9-19-O
b
LTM8-9-16-O
LTM8-9-14-G
LTM8-9-15-G
LTM8-9-17-O
δ18O‰
9.6 - 11.6
11.6 - 13.5
13.5 - 15.5
15.5 - 17.5
17.5 - 19.5
19.5 - 21.4
0 50 100 µm
c
a
a′
δ18O
OQ (overgrowth grain)
DQ (detrital grain)
distance from grain a (µm)
d
b
b′
δ18O
OQ (overgrowth grain)
DQ (detrital grain)
distance from grain b (µm)

(a)
Max (26.7‰)
Mean (18.5‰)
Min (7.5‰)
Pollington et al. (2016)
Sharp et al. (2016)
Clayton et al. (1972)
Kita et al. (1985)
Temperature (°C)
0
20
40
60
80
100
120
-20
-15
-10
-5
0
5
10
δ18Ofl ‰ VSMOW
(b)
Max (26.7‰)
Mean (18.5‰)
Min (7.5‰)
1
2
3
4
-20
-15
-10
-5
0
5
10
δ18Ofl ‰ VSMOW